Atmos. Meas. Tech. Discuss., 7, 11345–11378, 2014
www.atmos-meas-tech-discuss.net/7/11345/2014/
doi:10.5194/amtd-7-11345-2014

Atmospheric Measurement Techniques Discussions
Open Access

Reconstruction of 3-D cloud geometry using a scanning cloud radar

F. Ewald, C. Winkler, and T. Zinner

Meteorologisches Institut, Ludwig-Maximilians-Universität München, Theresienstr. 37, 80333 München, Germany

Received: 28 August 2014 – Accepted: 15 October 2014 – Published: 19 November 2014

Correspondence to: T. Zinner (tobias.zinner@lmu.de)

Published by Copernicus Publications on behalf of the European Geosciences Union.

Abstract

Clouds are one of the main reasons of uncertainties in the forecasts of weather and climate. In part, this is due to limitations of remote sensing of cloud microphysics. Present approaches often use passive spectral measurements for the remote sensing of cloud microphysical parameters. Large uncertainties are introduced by three dimensional (3-D) radiative transfer effects and cloud inhomogeneities. Such effects are largely caused by unknown orientation of cloud sides or by shadowed areas on the cloud. Passive ground based remote sensing of cloud properties at high spatial resolution could be improved crucially with this kind of additional knowledge of cloud geometry. To this end, a method for the accurate reconstruction of 3-D cloud geometry from cloud radar measurements is developed in this work. Using a radar simulator and simulated passive measurements of static LES model clouds, the effects of different radar scan resolutions and varying interpolation methods are evaluated. In reality a trade-off between scan resolution and scan duration has to be found as clouds are changing quickly. A reasonable choice is a scan resolution of 1 to 2°. The most suitable interpolation procedure identified is the barycentric interpolation method. The 3-D reconstruction method is demonstrated using radar scans of convective cloud cases with the Munich miraMACS, a 35 GHz scanning cloud radar. As a successful proof of concept, camera imagery collected at the radar location is reproduced for the observed cloud cases via 3-D volume reconstruction and 3-D radiative transfer simulation. Data sets provided by the presented reconstruction method will aid passive spectral ground-based measurements of cloud sides to retrieve microphysical parameters.

1 Introduction

Clouds strongly influence earth's radiation budget. Most radiative processes connected to clouds are extremely sensitive to cloud microphysics. Measurements of these processes are either direct but limited to small snippets, i.e., in-situ measurements from aircraft or they are indirect, i.e., from active or passive remote sensing. Remote sensing techniques are by themselves limited to spatial and temporal snapshots of the whole microphysical process within a cloud – but their advantages lies in their speed and in their mostly instantaneous acquisition of multidimensional datasets. For instance, an active cloud radar is well suited to derive cloud macrophysics (e.g. their 3-D geometry), but for the most part insensitive to small cloud droplets and therefore only provides limited information on cloud particle formation (Hobbs et al., 1985; Miller et al., 1998). On the other hand passive solar techniques can derive cloud particle characteristics very well (Nakajima and King, 1990; Twomey and Cocks, 1989), but only for the part of the cloud oriented towards sun and sensor.

For this reason the combination of different remote sensing techniques becomes increasingly important. In this work we describe one step towards such a combination: how an active cloud radar can provide the cloud geometry needed by passive techniques using reflected solar radiation.

Although this information is valuable for every passive technique, it is essential for techniques working on high spatial resolution. Cloud side remote sensing as proposed by Martins et al. (2011); Marshak et al. (2006) and Zinner et al. (2008) aims for the retrieval of vertical profiles of cloud microphysics from cloud edges observed from a ground, air or space perspective. Especially the complex-shaped cloud sides pose a problem for the passive retrieval of cloud microphysics at a spatial resolution of 100 m or less due to the unknown cloud surface orientation. In an effort to set up ground based cloud side remote sensing, the presented 3-D cloud reconstruction technique will alleviate the problem for the ground-based perspective if a cloud radar is available.

Not only this specific application but basically every remote sensing technique, especially passive, can benefit from such a volume reconstruction. The accuracy of satellite retrievals and their dependence on cloud geometry can be tested using cloud reconstructions. These volume reconstructions can furthermore serve as a validation dataset for cloud resolving modelling. Fielding et al. (2013) also use cloud radar data in order to consider cloud geometry in radiation closure studies.

Section 2 first introduces the theoretical toolbox used in the selection and development of the final reconstruction method. It is based on the combination of data from a high resolution cloud model, a simple radar simulator and simulations of cloud side imagery from the reconstructed cloud fields. Next, the actual development of the reconstruction method (Sect. 3) is described including the choice of scan strategies, the data remapping and interpolation and the correction for mean cloud motion. In Sect. 4 this approach is then subsequently applied to real-word cases. Finally, conclusions are drawn and the limitation posed by real-world cases due to cloud radar sensitivity are discussed.

2 Experiment setup

2.1 LES model test bed and radar simulator

The task of cloud volume reconstruction from scanning cloud radar starts with the question for the best scan strategy. Optimum scan speed and scan resolution have to be found as well as a suited method for the interpolation of the sparse and inhomogeneously distributed radar measurements into a contiguous cloud volume defined on a regular grid. In order to examine the influence of different scan resolutions and interpolation methods under controlled conditions, a simple radar simulator was developed allowing for the simulation of radar scans inside an artificial cloud field produced by a cloud resolving model. Data for a trade wind cumulus situation was used from the large-eddy-model of the University of California, Los Angeles (UCLA-LES) (Seifert and Heus, 2013). This data is well suited for the evaluation of cloud geometry reconstruction methods, because of its high spatial resolution of (25 m) in all three dimensions over a domain that spans 50 km × 50 km × 4 km. For the radar scan simulations, only a smaller 7.5 km × 7.5 km × 4 km part of the domain is selected, as illustrated in Fig. 1. The UCLA-LES cloud model provides liquid water mixing ratios which can be translated to a radar reflectivity factor z for each cloud box if a certain droplet radius r_0 is assumed.

Consider the radar reflectivity factor z in units of mm^6/m^3.

$$z = 2^6 \int_0^\infty N(r) r^6 \mathrm{d}r \tag{1}$$

With a constant droplet radius r_0, this simplifies to:

$$z = 2^6 N r_0^6, \tag{2}$$

where N stands for the number of particles per volume. Because values of Z can span many orders of magnitude they are normally expressed in form of the logarithmic radar reflectivity Z in units of dBZ:

$$Z = 10 \log_{10} \left(\frac{z}{1\,\mathrm{mm}^6/\mathrm{m}^3} \right). \tag{3}$$

The simulation of a radar scan is obtained from a single LES time step (at $t = 32\,\mathrm{h}$ simulation time), i.e., not only frozen turbulence assumption is applied but also the cloud motion is neglected during the radar scan.

Radar reflectivities Z are determined along a number of beams in radial distances from the radar with a cloud radar range gate length of 60 m. The scan pattern is determined by specifying a number of consecutive beam directions in terms of elevation and azimuth angles (Θ and Φ). This way measurement points in spherical coordinates are obtained. A ray tracer finds the LES grid box that contains each of the points. The radar reflectivity Z of this grid box is returned as simulated measurement value.

Additionally, an option to simulate finite radar sensitivity is included. If turned off, every Z value is accepted. Alternatively a threshold is used to set $z = 0$ for measurements smaller than a threshold. The distance-dependent threshold Z_{min} is set according to the minimal detectable radar reflectivity following Doviak and Zrnic (1993) and

Riddle et al. (2012):

$$Z_{\text{min}}(d) = C_0 + 10\log\left(\frac{\tau_0 P_{t_0}}{\tau P_t}\right) + 20\log\left(\frac{d + d_{\text{offset}}}{d_0}\right) + \text{SNR}_{\text{min}}[\text{dB}], \tag{4}$$

$$\text{SNR}_{\text{min}} = \frac{Q}{N_{\text{FFT}}\sqrt{K_{\text{avg}}}}. \tag{5}$$

Here, $C_0 = -20.7\,\text{dB}$ denotes the specific radar constant in logarithmic units for a reference distance of $d_0 = 5\,\text{km}$, a pulse duration of $\tau_0 = 200\,\text{ns}$, an average transmitter power of $P_{t_0} = 30\text{W}$ and including a 2 dB finite receiver bandwidth loss. The distance offset d_{offset} is used to shift the radar away from the cloud without a change of geometry. This way sensitivity can be analysed isolated from other changes due to a new measurement position. SNR_{min} is the minimal detectable signal-to-noise ratio which depends on the specific signal characteristics and its detection. During the scanning mode we incoherently averaged $K_{\text{avg}} = 10$ doppler spectra (totalling 0.5 sec) obtained from the Fast Fourier transformation ($N_{\text{FFT}} = 256$) of backscattered radar signals with a pulse length of $\tau = 400\,\text{ns}$ and an average transmitter power of $P_t = 52\text{W}$. In order to seperate signal and noise floor the method described by Hildebrand and Sekhon (1974) with a threshold $Q = 5$ was used. With this method a minimal SNR_{min} of about -22.1 dB can be reached if the signal power is contained within one FFT bin (Riddle et al., 2012).

Using Eq. (2)–(5) synthetic radar data is generated for a given cloud structure. In order to evaluate the quality of reconstruction possibilities for this structure a measure of success is needed.

2.2 Simulated cloud side images as quality measure

There seems to be no universal approach to quantify the accuracy of a volumetric reconstruction in literature. In any case, the metric should focus on the application and on the used property of the reconstructed cloud field. For example, Fielding et al. (2013)

AMTD
7, 11345–11378, 2014

were interested in radiative closure experiments and they therefore compared simulated fluxes at ground level. In contrast, in our study we are interested in a correct high resolution reconstruction of the cloud side facing the radar location to improve the retrieval of cloud microphysics using reflected solar radiation. Using simulated radiances from cloud sides in the solar spectral range is thus the most meaningful parameter of quality for our purpose.

To this end, a "photo" of the reconstructed cloud is simulated. The radiative transfer model MYSTIC is used, the Monte Carlo code for the physically correct tracing of photons in cloudy 3-D atmospheres (Mayer et al., 1998; Mayer, 2009). MYSTIC is part of the radiative transfer library libRadtran (Mayer and Kylling, 2005). For an arbitrary given cloud field, the corresponding observable radiance field can be derived with the MYSTIC "panorama" option (Mayer, 2009) if viewing position and field-of-view are defined. Radiance at a wavelength of $\lambda = 870\,\text{nm}$ is calculated for a range of solid angles and re-arranged into a "black and white photo" of the cloud as observable from the radar position. By means of these images reconstructed clouds can now be compared to the original cloud data from LES or to a real camera image.

This comparison can be conducted by human eye, a quite powerful instrument in order to detect reconstruction problems. A more objective way of comparison is the root mean square error of the radiance field based on reconstruction with the one from original LES data. This way a numeric expression for the deviation is provided.

Original LES data based radiance images can be generated from model LWC and a single fixed effective radius r_0. Figure 4a shows an example radiance image as observable from the radar simulator at the surface of the domain for the LES data. Each pixel is related to a pair of azimuth and elevation angles $[\Phi, \Theta]$ between 0 and 90° and 0 and 70°, i.e., the image is comparable to a wide-angle photo. In Fig. 4 the cloud side of the main cloud element is visible, illuminated from a sun zenith angle of 60° directly in the back of the sensor. The central cloud element is about 6.5 km wide and 3 km high (cf. Fig. 1). Apparently, additional clouds become visible towards the horizon due to periodic boundary conditions of the radiative transfer simulation.

AMTD
7, 11345–11378, 2014

Radar reflectivity factors z, simulated or measured, have to be converted back into cloud microphysical properties. As we are more concerned about geometry than about reproduction of exact microphysical properties, this step is simplified. This can be done because the actual choice of droplet size has a negligible influence on the radiance at 870 nm. Therefore a fixed cloud droplet radius r_0 is assumed throughout the cloud and thus the number concentration N in Eq. (2) can be replaced by the liquid water content LWC which then leads to

$$\mathrm{LWC}(z) = z \cdot \frac{\pi \cdot \rho_{\mathrm{H_2O}}}{48 \cdot r_0^3}. \tag{6}$$

Here $\rho_{\mathrm{H_2O}}$ is the density of water. For real measurements this approach involves some difficulties: drizzle and/or rain with high reflectivities within a cloud lead to unrealistic high values of LWC under the assumption of a fixed mono-disperse cloud droplet size r_0. As high LWC and therefore high optical thickness leads to an extremely large number of scattering events simulated by the Monte Carlo model, computational effort for the radiance simulation grows rapidly in these cases. For the sole effort of reconstructing the cloud geometry, quantitative values of microphysical fields are not crucial as long as the cloud objects are optically thick. Thus, a simple LWC cut-off at high values can be applied, equivalent to a certain maximum limit in z. The LWC field obtained this way is then basis of 3-D simulations providing radiance images to compare reconstruction and original cloud geometry.

2.3 The miraMACS cloud radar

Real radar measurements discussed here are obtained with the miraMACS cloud radar, a scanning ground-based 35 GHz, 8.4 mm-wavelength MIRA35-S cloud radar manufactured by METEK GmbH. It is located on the roof of the Meteorological Institute Munich as part of the Munich Aerosol Cloud Scanner project (MACS). It features full hemispheric scanning with scan speed up to $10^\circ\,\mathrm{s}^{-1}$. In Table 1, an overview of specifications of the miraMACS radar system is given. For the reconstruction of cloud

AMTD
7, 11345–11378, 2014

geometry, the effective radar reflectivity factors provided by the METEK data processing software were used (Bauer-Pfundstein and Görsdorf, 2007).

3 Development of reconstruction procedure

The procedure for cloud geometry reconstruction from radar measurements is illustrated in Fig. 2. Radar reflectivities collected during a scan are remapped from their original, spherical coordinates to Cartesian coordinates (distance from radar to the "east" (x), distance from radar to the "north" (y) and height above ground (z)). A correction of the horizontal wind drift is applied, based on radiosonde wind data. For the further application it is necessary to interpolate the inhomogeneously distributed measurements to a regular grid. This step concludes the reconstruction itself. This step is followed by the quality test (see Sect. 2.2), which consists of the comparison of a synthetic radiance image for the LES data, or a real camera picture recorded during the scan, and radiance simulations based on the reconstructed cloud volume. The individual steps and reconstruction parameters and methods analysed during testing are presented in more detail in the following.

3.1 Scan strategies

Scan pattern and scan resolution are the first parameters to be chosen. It turns out that for the reconstruction of isolated clouds the so called sector range-height-indicator (S-RHI) scan pattern is probably best suited. It consists of consecutive elevation scans for stepwise changing azimuths. This scan strategy allows best measurement of specific cloud side geometry for collocated near simultaneous passive spectral measurements. S-RHI is favoured over S-PPI (sector plane-parallel-indicator), a horizontal azimuth scan for stepwise changing elevation angle, because it can be used to partially correct for the cloud motion component tangential to the radar position.

AMTD
7, 11345–11378, 2014
3-D cloud geometry from scanning cloud radar
F. Ewald et al.

A second, critical question is the choice of the scan resolution. While high resolution leads to higher spatial accuracy, the scan takes more time and thus exhibits larger deviations from the ideal instantaneous, frozen cloud snapshot. The beam width of 0.6° defines the upper limit of the scan resolution. Figure 3b–f shows the results for the tests of different radar scan resolutions for the cloud situation shown in Fig. 1.

In this figure comparisons camera image simulations at 870 nm of LES based cloud reconstructions are shown for different scan resolutions between 1° and 5°. It can be seen in Fig. 3 that details of brightness gradients and general contrast of the data is widely lost at around 4° and above. Scans with resolutions coarser then approximately 2 to 4° have to be avoided as these scans do no longer allow detailed reconstruction. Detailed results of the root-mean-square error (RMSE) between interpolated and original cloud can be found in Table 2.

The specific trade-off between scan resolution and scan duration depends on the distance of the cloud (the larger the distance, the higher the angular resolution has to be) and the settings that determine the time to measure one profile (pulse repetition frequency, spectral averaging of spectra). In addition, the evolution time-scale and motion speed of a specific cloud has to be taken into account (turbulent convective vs. more static). In view of these constraints the scan resolution of a cloud radar can never reach the high spatial resolution of a passive imaging radiometer, which is only limited by sensor resolution and optics. For a cloud 5 km away the anticipated horizontal resolution of the front-facing cloud side lies in between 100–200 m. Choices for scan speed and scan resolution will be shown in Sect. 4 for specific applications on miraMACS data.

3.2 Remapping radar data to Cartesian space considering cloud motion

The measured data points are stored in spherical coordinates, the distance d from the radar together with the elevation angle (Θ) and the azimuth angle (Φ) of the beam. They are then remapped to Cartesian coordinates (x, y, z).

AMTD
7, 11345–11378, 2014

The time period for a scan with adequate resolution and scan speed is in the order of minutes. Depending on the atmospheric conditions, the cloud can change position significantly during this period. A complete consideration of this 3-D motion including turbulence is impossible. Nonetheless the main horizontal wind direction tangential to the radar position can be corrected. To this end the wind profile from a nearby atmospheric sounding can be used. Let t_0 be the central time of a scan period. Each radar measurement has a time t_i and a location $(x(t_i), y(t_i), z(t_i))$. According to the wind speed u in x direction and v in y direction taken from a radiosonde profile, $x(t_i)$ and $y(t_i)$ are shifted to their approximate position at time t_0 (using $z(t_i)$ to select best vertical level in the sounding):

$$x(t_0) \approx x(t_i) + u \cdot (t_0 - t_i) \tag{7}$$

$$y(t_0) \approx y(t_i) + v \cdot (t_0 - t_i). \tag{8}$$

Thus, early measurements are shifted downwind, later measurements upwind.

3.3 Interpolation methods

The interpolation of the scattered radar data on a dense regular grid is the central reconstruction step. The reconstructed LWC field is necessary for all subsequent steps (radiance simulation, 3-D display of the cloud, application in passive cloud side remote sensing).

The sparse and inhomogeneously distributed data makes the interpolation challenging. In addition, the sensitivity limit with respect to small cloud droplets leads to some uncertainty in the definition of cloud boundaries. In order to consider these challenges, several interpolation methods and parameters were tested in the controlled environment of the LES cloud case: nearest-neighbour interpolation, Shepard method (Shepard, 1968), barycentric interpolation (Möbius, 1976), and natural neighbour interpolation (Sambridge et al., 1995). The results of all methods when applied to the same, synthetic measurement are shown in Fig. 4.

AMTD
7, 11345–11378, 2014

From the visual impression of Fig. 4, some disadvantages of the different interpolation methods are already visible. The nearest-neighbour interpolation (Fig. 4a) produces box structures which become clearly visible when doing 3-D radiative transfer calculations. Though smoother in appearance the Shepard method leads to several artefacts as well, which are caused by its tendency to include data points further away. By eye, the deviation in radiance fields of the reconstructed cloud compared to the original model cloud seems lowest for barycentric and natural neighbour interpolation. The root-mean-square errors (RMSE) between the radiance fields of the reconstructed cloud and the original cloud does not clearly show these differences (see Table 3).

The interpolation artefacts can be seen more clearly in the liquid water content field. In Fig. 5 a horizontal cross-section (Fig. 5a) of an artificial cloud was sampled using the spatial resolution of the proposed S-RHI scan pattern (Fig. 5b). The following panels (Fig. 5c–f) show the results of the different interpolation methods. The grid box structure (Fig. 5d) of the nearest-neighbour method and the ripple pattern (Fig. 5e) of the Shepard method in-between the radar beams strongly distort the shape of the cloud boundary. In contrast the barycentric (Fig. 5f) and natural neighbour interpolation (Fig. 5c) yield very similar results. Both methods give a good reconstruction of the shape of the cloud boundary and the overall liquid water content field. Both of them tend to result in a slightly blurry reconstruction, especially at the cloud edges.

A more comprehensive analysis of the different methods can be made when the LWC fields are compared in the frequency domain. In Fig. 6 the power spectral density (PSD) of the LWC fields are shown for the different reconstruction methods when given the radar data with a scan resolution of 2°. Naturally, all reconstructed LWC fields fall short in reproducing the small scale LWC fluctuations. While the nearest-neighbour method produces too strong gradients, the returned fields for all other interpolation methods are too smooth. This behaviour becomes dominant at scales below the spatial sampling frequency (which varies between 50–250 m as a function of the radial distance). The natural neighbour interpolation field becomes too smooth while the barycentric and Shepard method reproduce the original PSD the best. Since the Shepard method did

AMTD
7, 11345–11378, 2014

not perform as well as the other two methods in the reconstruction of the radiance field (Fig. 4) and also showed problematic artefacts in the synthetic LWC field (Fig. 5) it is not taken into consideration. The tendency of the natural neighbour method to produce fields which are too smooth becomes more pronounced towards the 5° scan resolution. This is shown in Fig. 7 where the variation of the PSD between 1–5° is plotted for the natural neighbour (red) and barycentric (green) method. It is evident that the PSD for the barycentric interpolation is less affected by scan resolution compared to the PSD for the natural neighbour interpolation.

Following these findings and due to its superior numerical stability (Berrut and Trefethen, 2004; Higham, 2004) the barycentric interpolation is chosen here. In the following, the S-RHI scan strategy with a resolution of 1 to 2° and the barycentric interpolation is used to reconstruct the 3-D cloud geometry.

3.4 Sensitivity to detection threshold

In cloud radar science there is always the question to which extent cloud boundaries measured by radar are equivalent to the ones found by optical means, e.g., lidar or human eye. This can be explained with the low sensitivity with respect to small droplets and to small droplet number concentrations (see Eq. 2). This leads to microwave signals which are too small to be detected, even though the backscattered signal at shorter, optical wavelengths is well measurable.

For a radar scan leading to a successful cloud geometry reconstruction, certain microphysical conditions have to be met. To this end, some further studies were conducted for the LES cloud data. As before, the radar simulator was situated in the lower left corner, but this time with varying values of droplet radius (r_0 which affects the radar reflectivities (Eq. 2) and a varying distance between radar and cloud. All simulated radar scans were performed with 2° resolution in elevation and azimuth angle. Interpolation is done with the barycentric neighbour method. In Fig. 8 results are shown for r_0 ranging from 1 to 10 µm and for a distance between radar and closest cloud side of about 3 (top) and 10 km (bottom). As one would expect from Eq. (2), the cloud is

AMTD
7, 11345–11378, 2014

detected better the larger the droplets are and the closer the cloud is situated to the radar site. In our case this is reflected by the number of cloud boxes which lie above a particular detection threshold (also see Table 4). This number decreases with rising sensitivity threshold. If a relative loss of 10 % of detected cloud boxes compared to a measurement with an ideal radar is defined as an acceptable limit, the required droplet radius is 3 µm (resp. 5 µm) for a distance of 3 km (resp. 10 km). These simplified values should provide a guide line for the assessment of the following real reconstruction cases. Several additional limitations affect the realistic estimation of detection thresholds in reality. The detection threshold as defined in Eq. (4) is therefore only the upper boundary of the sensitivity a perfect radar would exhibit. Atmospheric absorption and broadening of the Doppler spectrum due to turbulence attenuate the signal power received in each velocity bin inside the receiver.

4 Application of the cloud reconstruction method

Reconstruction of convective clouds

So far, presented results and arguments are all based on synthetic data only. In the following, application of the reconstruction technique to real data will be shown. Two different cases illustrate possibilities and limitations. Both have been measured during the summer season of 2013 with the miraMACS cloud radar on the roof of the Meteorological Institute in the centre of Munich.

The first demonstration case is based on a radar scan which was collected on 30 July 2013, 09:17–09:21 UTC. During the scan, a picture of the cloud was recorded by a camera, which is mounted on the radar and points in beam direction (Fig. 9, left). The scan covered an azimuth range of 20° and an elevation range of 16°. From left to right (i.e., north to south) 15 range height indicators (RHI) were scanned leading to an azimuth resolution of about 1.3°. The scan speed was $1^{\circ}\,s^{-1}$ which corresponds to a duration of about 4 min to scan the whole cloud. In combinration with an averaging

AMTD
7, 11345–11378, 2014

Title Page
Abstract Introduction
Conclusions References
Tables Figures
◀◀ ▶▶
◀ ▶
Back Close
Full Screen / Esc
Printer-friendly Version
Interactive Discussion

time of 0.5 s, this results in a 0.5° resolution in elevation direction. A simple estimation for the spatial resolution (Δr) in dependence of the distance d to the radar and the resolution in degree $\Delta\alpha$ is given by $\Delta r = 2 \cdot d \cdot \sin(\Delta\alpha)$. With the closest cloud side at a distance of about 13 km to the radar, this leads to a resolution of about 300 m in azimuth and about 110 m in elevation direction. The radial resolution (determined by the radar range gate length) is 60 m.

Applying the described method (Sect. 3), a field of regularly spaced ($\Delta x = \Delta y = \Delta z = 100$ m) z values was reconstructed. These radra reflectivity factors were converted to a field with values of LWC and droplet radius according to Sect. 2.2. This time the droplet radius was set constant to $r_0 = 7.5\,\mu$m, the Z_e-cut-off was chosen to be at −25 dBZ, corresponding to a maximal LWC of 0.35 g m^{-3}. A MYSTIC 3-D simulation provides a colour image (by simulating red, green and blue channels, Fig. 9, right) with field-of-view and spatial resolution matching the resolution of the installed camera. The images compare reasonably well (cf. Fig. 9, right).

The second case that is presented here is based on a scan on 25 July 2013 that took place between 15:23–15:27 UTC. This scan covered a range of 30° in azimuth and 28° in elevation direction (see camera picture in Fig. 10, left) and took about 4 min to scan the cloud. With a scan speed of 2° s^{-1} and an averaging time of 0.5 s, a resolution of 1° was reached on the elevation axis. On the azimuth axis, also a 1° resolution was obtained. Since the wind speed was much higher on this day the cloud motion correction was even more important. The distance of the cloud, between 17 and 27 km, was partly beyond the range of the radar. Interpolation was done at an equidistant 100 m grid, leading to a field of Z_e values and related microphysical parameters (r_0 = 7.5 µm, Z_e-cut-off at −25 dBZ, max. LWC = 0.35 g m^{-3}). The observed and simulated radiance image is shown in Fig. 10. The result again compares well to the camera picture.

As the radar provides unique capabilities, it is impossible to get a more objective verification for these reconstruction results. Nevertheless, for the intended application in combination with passive cloud side observations, the presented tool shows promising

AMTD
7, 11345–11378, 2014

results. As the camera picture is similar to cloud side imagery a predominant agreement in this respect is a significant result.

5 Summary and discussion

A method for the reconstruction of cloud geometry from cloud radar scans was presented. In this study the method has been developed with the aim to provide cloud geometry information. This is needed for the analysis of solar radiation reflected by clouds sides with respect to retrievals of cloud microphysics. By combining geometrical and radiative inputs cloud sides become accessible for passive remote sensing applications. The volumetric cloud reconstruction essentially consists of three steps:

1. Using a sector range-height-indicator scan, radar data for a specific cloud is collected. This scan pattern allows for targeted observations of individual cloud sides and for simple correction of mean tangential wind. Vertical slices of radar data, collected in consecutive steps are shifted horizontally to compensate for the mean wind direction during the scan. Central to this scan strategy is the choice of a scan resolution. This choice is situation dependent. For a static cloud scene, results would obviously be best with a high spatial resolution (with the radar beam width as the upper limit). On the other hand, for averaging times ranging from tenths of a second to seconds for a single radar profile, high spatial resolution leads to considerable scan durations. Cloud motion, convection and turbulence quickly change the cloud volume and therefore scan duration should be kept as short as possible. Resolutions between 0.5 and 2° are a reasonable compromise in order to reach a spatial resolution of about 100–200 m at cloud surface.

2. After the measurement, a first order correction of the horizontal wind drift is done. Radiosonde wind profiles are used to adjust measurement positions according to their collection time.

AMTD
7, 11345–11378, 2014

3. The subsequent interpolation of the scattered measurements from the consecutive radar profiles on a regular 3-D grid turns out to be challenging, due to the data sparseness. Different interpolation methods were examined. Among the tested interpolation methods (nearest-neighbour, Shepard method, barycentric interpolation and natural neighbour interpolation), the barycentric interpolation scheme yields the best result.

These steps were tested by means of a synthetic test bed of simulated cloud data from an LES model (the "truth"), cloud side radiance images (cloud "photos" parallel to the radar observation as quality measure), and derived radar scan data. The latter step assumes stationarity and a simplified conversion of equivalent radar reflectivity into microphysical parameters. On this synthetic radar data the techniques were applied to find necessary spatial (angular) resolution and best interpolation technique. Quality of reconstruction is always examined based on a comparison of simulated cloud side radiance images of true and reconstructed cloud geometry.

The reconstruction of 3-D cloud geometry is based on radar measurements which have their own set of limitations which are not main object of this work, but have to be considered. Situations exist when a cloud volumes radar reflectivity is below the radar sensitivity threshold. To characterise the microphysical situation in which radar data allows for reasonable reconstruction, the LES based radar simulations including an approximation of the radar detection threshold were used (Eq. 4). Based on given estimates from Metek GmbH[1] of the sensitivity of the miraMACS cloud radar, a minimum droplet radius of 3 µm (resp. 5 µm) for a cloud distance of 3 km (resp. 10 km) is required for a successful reconstruction. In reality the droplet radius even needs to be larger due to the broadening of the Doppler-spectrum caused by turbulence. The theoretical threshold values can be calculated for individual velocity bins lying within the receiver bandwidth corresponding to the inherent receiver noise characteristics. When

[1] Specification sheet available at http://metekgmbh.dyndns.org/mira36x.html.

turbulence causes differential radial velocities between cloud droplets the backscattered signal power gets spread over multiple velocity bins of the receiver bandwidth.

Through these limitations parts of the cloud volume stay undetected by the standard radar processing schemes. In some cases whole clouds are invisible to the radar at Munich. For example, this is the case for freshly formed cumuli and rather aerosol burdened situations, both facts leading to small droplets. Especially for the pure cloud detection and geometry reconstruction necessary for the presented methods, sensitivity could probably be improved if data quality requirements needed for more advanced evaluations are relaxed. Nonetheless, for specific cases reconstruction is successfully working, as presented for two cases of convective clouds. A comparison between the reconstructed clouds, in the form of simulated radiance images, and real pictures recorded during the scans show clear similarity of the lateral cloud edge contours as well as of 3-D features oriented towards the ground observations.

Thus, the planned combination with hyperspectral images of cloud sides in the Munich Aerosol Cloud Scanner project (MACS) may soon yield profiles of microphysical quantities.

Acknowledgements. We would like to thank Axel Seifert for providing the UCLA cloud model fields and Matthias Bauer-Pfundstein for helpful discussions on cloud radar sensitivity.

References

Bauer-Pfundstein, M. and Görsdorf, U.: Target separation and classification using cloud radar Doppler-spectra, in: Proceedings 33rd Intern. Conf. on Radar Meteorology, Cairns, Australia, 2007. 11353

Berrut, J. and Trefethen, L.: Barycentric Lagrange Interpolation, SIAM Rev., 46, 501–517, doi:10.1137/S0036144502417715, 2004. 11357

Doviak, R. J. and Zrnić, D. S.: Doppler Radar and Weather Observations, Dover Publications, 1993. 11349

Fielding, M. D., Chiu, J. C., Hogan, R. J., and Feingold, G.: 3D cloud reconstructions: evaluation of scanning radar scan strategy with a view to surface shortwave radiation closure, J. Geophys. Res.-Atmos., 118, 9153–9167, doi:10.1002/jgrd.50614, 2013. 11347, 11350

Higham, N. J.: The numerical stability of barycentric Lagrange interpolation, IMA J. Numer. Anal., 24, 547–556, doi:10.1093/imanum/24.4.547, 2004. 11357

Hildebrand, P. H. and Sekhon, R. S.: Objective Determination of the Noise Level in Doppler Spectra, J. Appl. Meteorol., 7, 808–811, doi:10.1175/1520-0450(1974)013<0808:ODOTNL>2.0.CO;2, 1974. 11350

Hobbs, P. V., Funk, N. T., Weiss, R. R., Locatelli, J. D., and Biswas, K. R.: Evaluation of a 35 GHz radar for cloud physics research, J. Atmos. Ocean. Tech., 2, 35–48, doi:10.1175/1520-0426(1985)002<0035:EOAGRF>2.0.CO;2, 1985. 11347

Marshak, A., Martins, J. V., Zubko, V., and Kaufman, Y. J.: What does reflection from cloud sides tell us about vertical distribution of cloud droplet sizes?, Atmos. Chem. Phys., 6, 5295–5305, doi:10.5194/acp-6-5295-2006, 2006. 11347

Martins, J. V., Marshak, A., Remer, L. A., Rosenfeld, D., Kaufman, Y. J., Fernandez-Borda, R., Koren, I., Correia, A. L., Zubko, V., and Artaxo, P.: Remote sensing the vertical profile of cloud droplet effective radius, thermodynamic phase, and temperature, Atmos. Chem. Phys., 11, 9485–9501, doi:10.5194/acp-11-9485-2011, 2011. 11347

Mayer, B.: Radiative transfer in the cloudy atmosphere, European Physical Journal Conferences, 1, 75–99, 2009. 11351, 11377

Mayer, B. and Kylling, A.: Technical note: The libRadtran software package for radiative transfer calculations – description and examples of use, Atmos. Chem. Phys., 5, 1855–1877, doi:10.5194/acp-5-1855-2005, 2005. 11351

Mayer, B., Kylling, A., Madronich, S., and Seckmeyer, G.: Enhanced absorption of UV radiation due to multiple scattering in clouds: experimental evidence and theoretical explanation, J. Geophys. Res., 103, 31241–31254, 1998. 11351

Miller, M. A., Verlinde, J., Gilbert, C. V., Lehenbauer, G. J., Tongue, J. S., and Clothiaux, E. E.: Detection of nonprecipitating clouds with the WSR-88D: a theoretical and experimental survey of capabilities and limitations, Weather Forecast., 13, 1046–1062, doi:10.1175/1520-0434(1998)013<1046:DONCWT>2.0.CO;2, 1998. 11347

Möbius, A. F.: Der baryzentrische Calcul, Georg Olms Verl., Hildesheim, original Edn., Leipzig, Germany, 1827, 1976. 11355

AMTD

7, 11345–11378, 2014

Nakajima, T. Y. and King, M. D.: Determination of the optical thickness and effective particle radius of clouds from reflected solar radiation measurements. Part I: Theory, J. Atmos. Sci., 47, 1878–1893, 1990. 11347

Riddle, A. C., Hartten, L. M., Carter, D. A., Johnston, P. E., and Williams, C. R.: A minimum threshold for wind profiler signal-to-noise ratios, J. Atmos. Ocean. Tech., 29, 889–895, doi:10.1175/JTECH-D-11-00173.1, 2012. 11350

Sambridge, M., Braun, J., and McQueen, H.: Geophysical parametrization and interpolation of irregular data using natural neighbours, Geophys. J. Int., 122, 837–857, 1995. 11355

Seifert, A. and Heus, T.: Large-eddy simulation of organized precipitating trade wind cumulus clouds, Atmos. Chem. Phys., 13, 5631–5645, doi:10.5194/acp-13-5631-2013, 2013. 11348, 11369

Shepard, D.: A two-dimensional interpolation function for irregularly-spaced data, in: Proceedings of the 1968 23rd ACM National Conference, ACM'68, New York, USA, doi:10.1145/800186.810616, 517–524, 1968. 11355

Twomey, S. and Cocks, T.: Remote sensing of cloud parameters from spectral reflectance in the near-infrared, Beiträge zur Physik der Atmosphäre, 62, 172–179, 1989. 11347

Zinner, T., Marshak, A., Lang, S., Martins, J. V., and Mayer, B.: Remote sensing of cloud sides of deep convection: towards a three-dimensional retrieval of cloud particle size profiles, Atmos. Chem. Phys., 8, 4741–4757, doi:10.5194/acp-8-4741-2008, 2008. 11347

AMTD
7, 11345–11378, 2014

3-D cloud geometry from scanning cloud radar

F. Ewald et al.

Table 1. Technical specifications and operational parameters of the miraMACS cloud radar. If two values are given, the first one is used in vertical viewing mode, the one labelled with an asterisk is used in scan mode. PRF is the pulse repetition frequency, N_{FFT} the number of consecutive pulses used for one Doppler spectrum.

Parameter	Value
Model	METEK MIRA-35S
Frequency	35 GHz
Wavelength	8.4 mm
Beam width	$0.6^{\circ} \times 0.6^{\circ}$
Peak power	30 kW
PRF	5 kHz
N_{FFT}	256
Incoherent averages	200, 10*
Vertical Resolution	30, 60* m
Sensitivity (best case) in 5 km	−48.8, −48.3* dBZ

AMTD
7, 11345–11378, 2014

Table 2. Measure of reconstruction quality for different scan resolutions. Root mean square errors (RMSE) in $\mathrm{mW\,m^{-2}\,sr^{-1}\,nm^{-1}}$ of simulated radiance fields from reconstructed clouds (Fig. 3b–f) compared to the original LES cloud ("the truth", Fig. 3a).

resolution	RMSE*
$1^\circ \times 1^\circ$	20.6
$2^\circ \times 2^\circ$	25.0
$3^\circ \times 3^\circ$	28.5
$4^\circ \times 4^\circ$	32.3
$5^\circ \times 5^\circ$	34.4

* $\mathrm{mW\,m^{-2}\,sr^{-1}\,nm^{-1}}$.

AMTD
7, 11345–11378, 2014

Table 3. Measure of reconstruction quality for different interpolation methods. Root mean square errors (RMSE) in $mW\,m^{-2}\,sr^{-1}\,nm^{-1}$ of simulated radiance fields from reconstructed clouds (Fig. 4a–d) compared to the original LES cloud ("the truth", Fig. 3a).

method	RMSE*
nearest-neighbour	21.9
Shepard	21.0
barycentric	21.1
natural neighbour	20.3

* $mW\,m^{-2}\,sr^{-1}\,nm^{-1}$.

AMTD
7, 11345–11378, 2014

3-D cloud geometry from scanning cloud radar

F. Ewald et al.

Table 4. Loss of detected cloud boxes due to radar detection threshold compared to an ideal radar in a simulated cloud (false negatives). Different values of droplet radii (r_0) are assumed for Z_e calculation. (d_{offset}) determines the distance between radar and cloud side in the calculation of the detection threshold. In total 12 155 cloud boxes could be detected by an ideal cloud radar.

r_0 (µm)	loss of detected boxes compared to ideal radar (%)	
	$d_{offset} = 0$ km	$d_{offset} = 7$ km
1.0	69.4	100
2.0	18.7	74.2
3.0	7.1	34.2
4.0	3.3	17.0
5.0	1.7	9.4
6.0	1.1	5.8
7.0	0.67	3.8
8.0	0.39	2.7
9.0	0.26	1.9
10.0	0.19	1.43

AMTD
7, 11345–11378, 2014

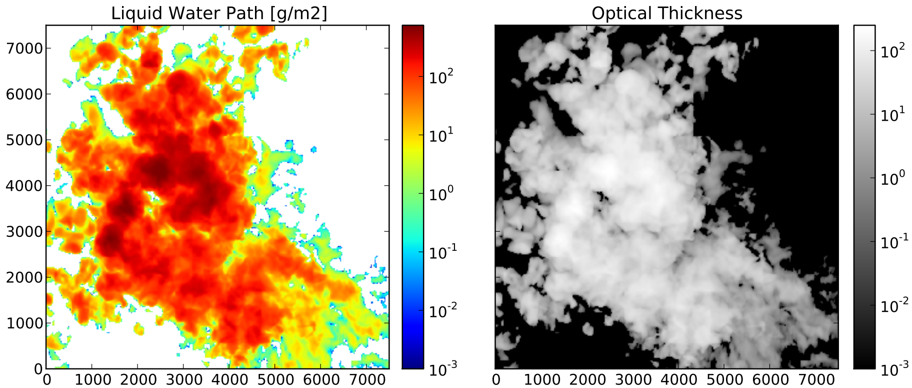

Figure 1. (left) Liquid water path (LWP) of the 7.5 km × 7.5 km domain of a trade wind cumuli large eddy simulation that was used to test the radar reconstruction under controlled conditions. The radar simulator was positioned in the lower left corner. (right) Optical thickness for the same cloud scene. The cloud field data is taken from (Seifert and Heus, 2013).

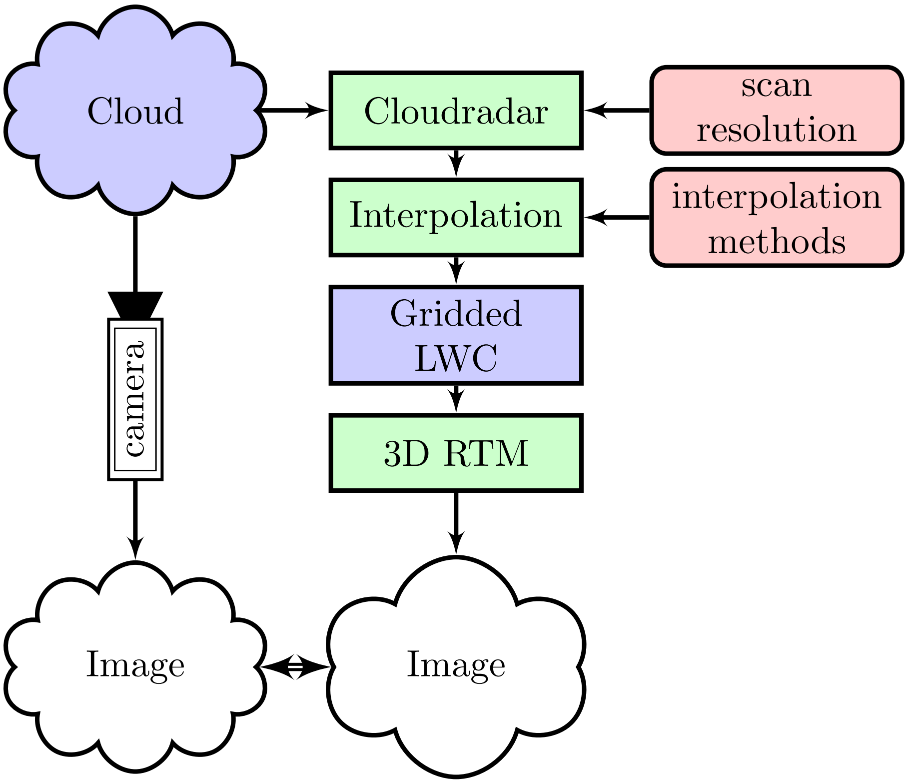

Figure 2. Illustration of the process chain leading from a radar scan to the 3d cloud reconstruction. Influence of scan resolution and interpolation method is analysed by the comparison of the simulated cloud field and the camera picture of the original cloud.

AMTD
7, 11345–11378, 2014

3-D cloud geometry from scanning cloud radar

F. Ewald et al.

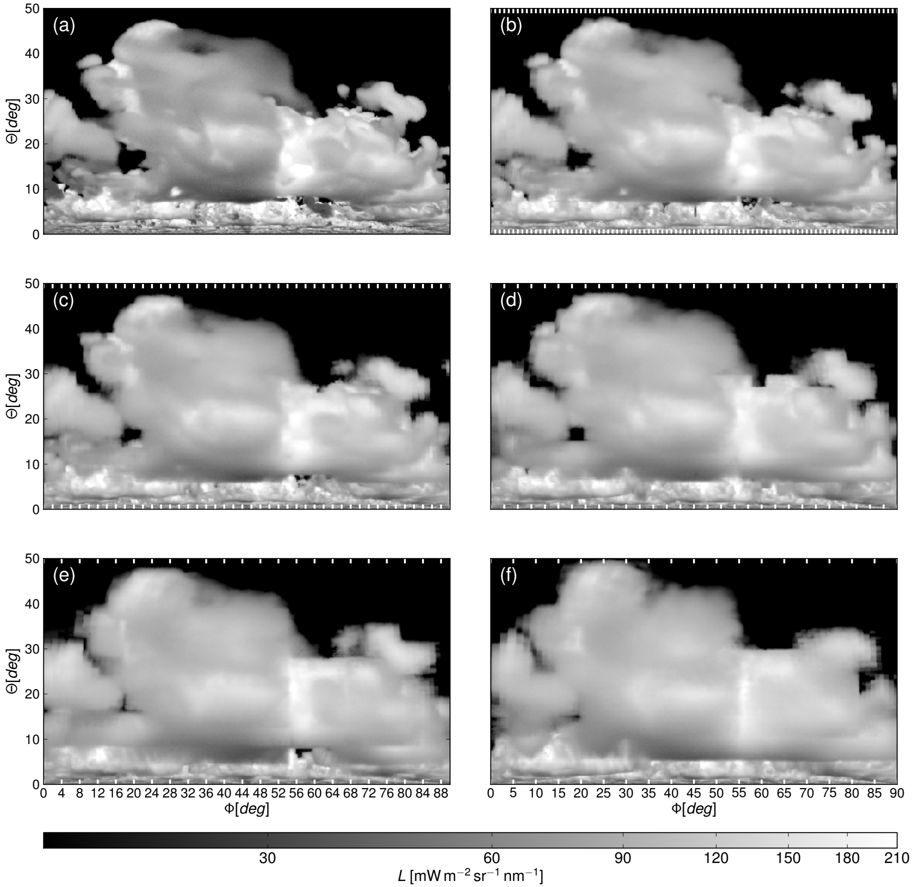

Figure 3. Comparison of reconstruction result for different scan resolutions. **(a)** shows the "true" high resolution radiance panorama at 870 nm. Other panels show the radiance panorama for reconstructions at elevation and azimuth angle resolution of: **(b)** 1°, **(c)** 2°, **(d)** 3°, **(e)** 4°, **(f)** 5°. Interpolation method is barycentric (cf. Fig. 4).

AMTD
7, 11345–11378, 2014

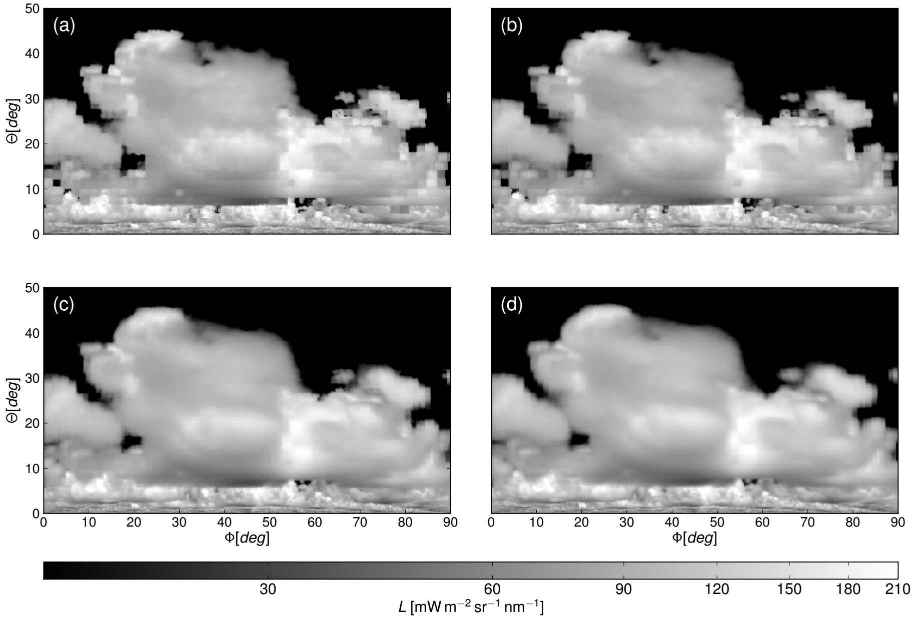

Figure 4. Comparison of reconstruction results for different interpolation methods on the basis of the high resolution radiance field at 870 nm. Results are shown for **(a)** the nearest-neighbour, **(b)** Shepard, **(c)** barycentric, **(d)** and natural neighbour interpolation when applied to 2° scan data.

AMTD
7, 11345–11378, 2014

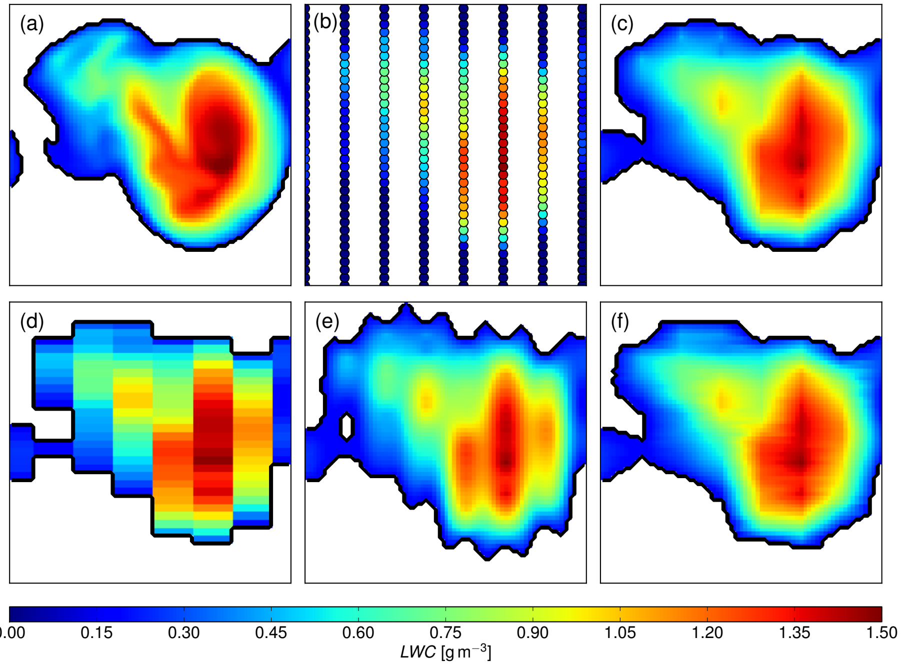

Figure 5. Illustration of different interpolation techniques and corresponding artefacts: **(a)** Shows the “true“ liquid water content field used, **(b)** represents scan resolution chosen for these interpolation tests. The artifical measurements in **(b)** were then used to reconstruct the original LWC field using **(c)** natural neighbour, **(d)** nearest-neighbour, **(e)** Shepard and **(f)** barycentric interpolation (cf. Fig. 4).

AMTD
7, 11345–11378, 2014
3-D cloud geometry from scanning cloud radar
F. Ewald et al.

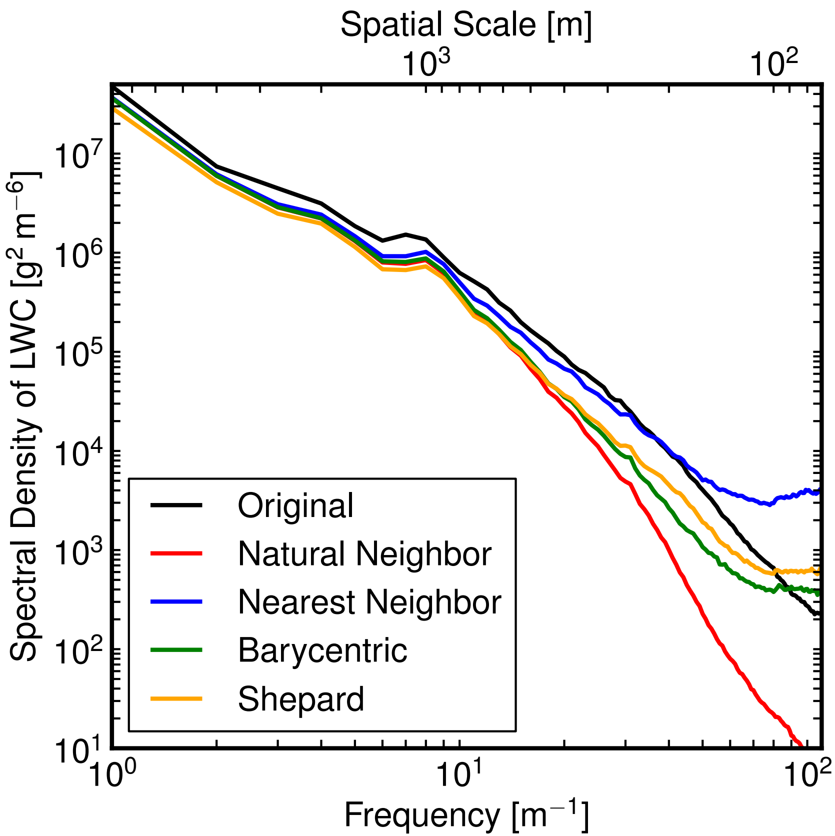

Figure 6. Comparison of Power Spectrum Density of the reconstructed liquid water content fields (compare Fig. 4) for different interpolation methods. The black line shows the Power Spectral Density (PSD) for the "true" LWC field. The other lines show the PSD for the reconstructions using the nearest-neighbour (blue), Shepard (yellow), barycentric (green) and natural neighbour (red) interpolation (cf. Fig. 4).

AMTD
7, 11345–11378, 2014

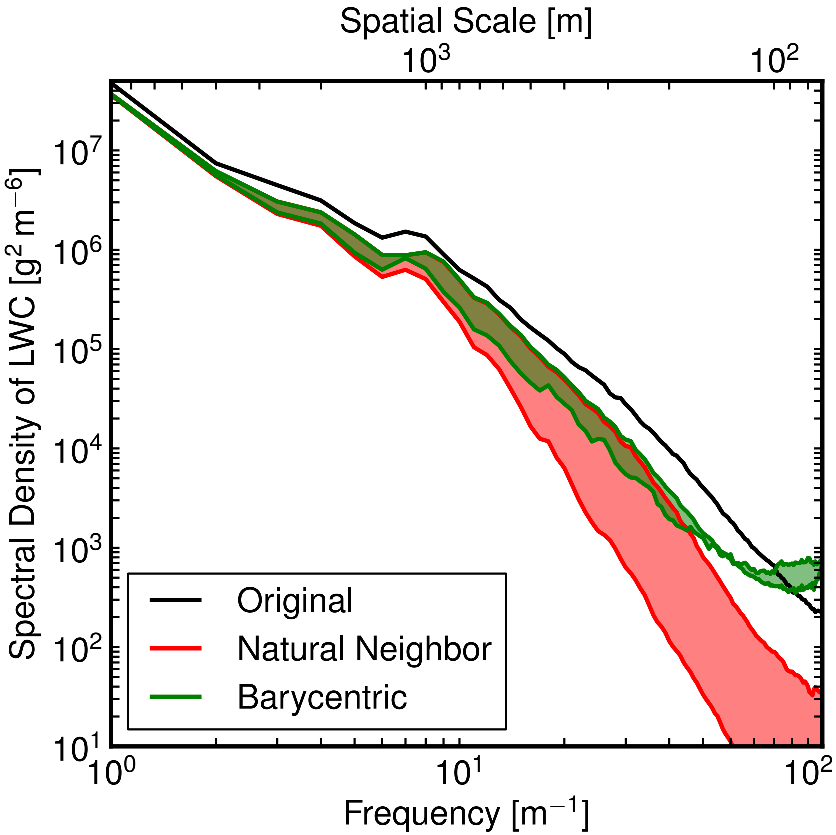

Figure 7. Comparison of the variability of the Power Spectrum Density of the reconstructed liquid water content fields (compare Fig. 4) with different scan resolutions. The black line shows the Power Spectral Density for the "true" LWC field. The green shaded area encloses the PSDs of the barycentric interpolation between 1 and 5° scan resolution. The red shaded area encloses the PSDs of the natural neighbour interpolation between 1 and 5° scan resolution (cf. Fig. 3).

AMTD
7, 11345–11378, 2014

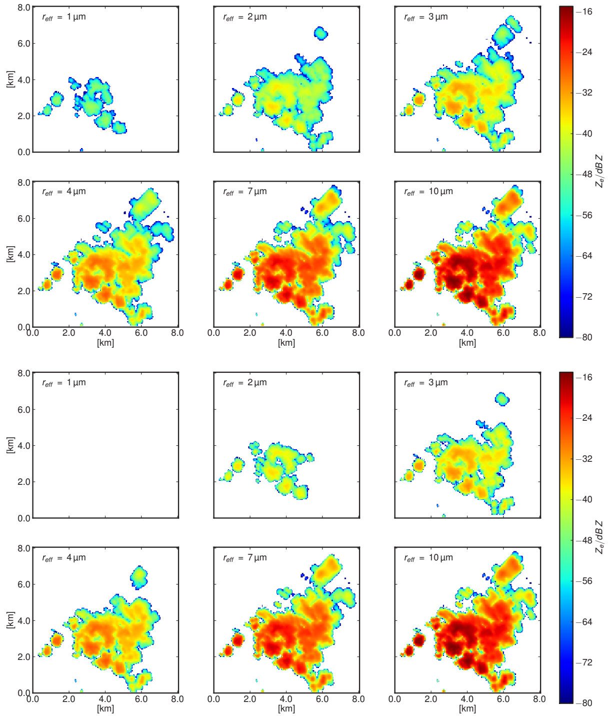

Figure 8. A horizontal slice through the reconstructed volume of equivalent radar reflectivities (height = 1.7 km) shows the influence of the radar sensitivity limit on the reconstruction result. The figure illustrates the radar sensitivity limit as a function of the cloud droplet radius and the distance between the cloud and the radar. The fixed cloud droplet radius is varied from 1 to 10 µm between the panels while the LWC is held constant. In the first six panels the radar simulator is situated at $x = y = 0$ km while in the last six panels the radar was moved further away at $x = y = -7$ km to illustrate the influence of the cloud-to-radar distance on the reconstruction result.

AMTD
7, 11345–11378, 2014

Figure 9. (left) Picture of a convective cloud taken during a miraMACS S-RHI scan (30 July 2013, 09:19 UTC. (right) Reconstruction result for the scan from figure on the left. The picture was simulated using MYSTIC Monte Carlo model (Mayer, 2009). Smaller clouds in the background are caused by the periodic boundary conditions which were used in the Monte-Carlo simulation.

AMTD
7, 11345–11378, 2014

Figure 10. (left) Picture of a convective cloud taken during a miraMACS S-RHI scan (25 July 2013, 15:24 UTC). (right) Reconstruction result for the scan from figure on the left. The picture was simulated using MYSTIC.

Discussion Paper | Discussion Paper | Discussion Paper | Discussion Paper |

AMTD

7, 11345–11378, 2014

3-D cloud geometry from scanning cloud radar

F. Ewald et al.